Performance Impact of Solar Gain on Photovoltaic Inverters and Utility-Scale Energy Generation Systems

Kenneth M. Armijo

Sandia National Laboratories, Albuquerque, NM 87185 USA

***Abstract* — Accurate performance and reliability evaluation of utility-scale photovoltaic (PV) systems requires accountability of solar gain contributions. A novel solar gain utility-scale inverter model has been developed to characterize inverter efficiency with respect to solar resource, general ambient conditions and thermal system losses. A sensitivity analysis was performed to evaluate the robustness of the model based on four assumed material properties. This analysis revealed 22.9% modeled internal inverter temperature sensitivity to surface absorptivity, with significantly less sensitivity to other parameters studied, indicating the impact of proper surface coating material selection on solar thermal absorption. This analysis was applied to a large utility-scale PV plant, assessing performance data from twelve 500kW inverters, and environmental data from twelve respective meteorological test stations. An RMSE value of 6.1% was found between the model and measured inner inverter temperatures. The results also suggest a negative $3.6x10^{-4}$ $[W/m^2]^{-1}$ normalized inverter efficiency correspondence with solar gain heat adsorption across the twelve inverters for a one-day, clear-sky time period.**

***Index Terms*—Solar gain, inverter, photovoltaics, utility-scale PV plant.**

I. Introduction

Increased PV utility-scale plant development in varying geographic locations has required the need for enhanced thermal characterization, especially for plants in high solar resource and temperature environments. As the level of solar radiation increases, so too does the level of solar gain heating, defined as the difference between incident energy and thermal losses. The results of this investigation will help address the impact of solar gain on internal inverter temperatures, which directly impacts the performance and reliability of an inverter. This can be particularly true with regard objects comprised of large thermal inertia. Optimal thermal management has been shown to not only be vital for PV modules, but also for inverters and other balance of system (BOS) components [1]. In particular, PV inverter system performance has been shown to vary with solar concentration, with respect to global horizontal irradiance (GHI) as well as temperature [2]. Catelani et. al. [3] demonstrated through inverter laboratory and field test measurements, the temperature sensitivity these systems have with respect to performance, especially with regard to power electronics. Smet et. al. [4] and Berning et. al. [5] provided evidence indicating the detrimental effects that high operating temperatures, especially above 50°C, have in creating thermal stress that can impact switching performance of integrated bipolar gate transistors (IGBT). Zhang et. al. [7] studied the performance of large grid-connected PV power systems and found that an inverter's reliability reduced with temperature and reported an available energy generation index reduction of 3% due to temperatures reaching 60°C. Finally, PV reliability studies by Sorensen et. al. [1] and He et. al. [8] provided accumulated damage evidence of various inverter components that were thermally stressed, not just by electric current heating, but due to ambient heat transfer contributions as well.

Studies have also examined solar irradiance variation impacts on utility-scale PV modules and inverter systems. These studies, such as those from Marion et. al. [8] and Stein [2] addressed cloud cover ramp rates on grid stability and plant energy generation. These respective studies found that the correlation between irradiance and distance across a site decreased as the site becomes larger, and they found a reduction in PV system efficiency as the ambient temperature increased beyond 25°C. Marion et. al. [8] investigated PV energy generation performance parameters for PV plants in varying sizes and locations. The authors indicated a strong potential dependence of a performance ratio, defined as actual output energy to ideal energy generation on ambient temperature for a large solar facility in Boulder, Colorado. At this location, over a 30 year period, the performance ratio was found to vary by as much as 17% between cold and warm weather months.

Although prior studies have investigated the impact of solar irradiance variability on PV generation effects [14-16], as well as temperature assessments of PV modules and solar heat collectors [1], few studies have addressed the impacts of solar gain contributions on performance and reliability of utility-scale PV inverter systems. This investigation evaluates PV inverter performance and thermal impacts due to solar gain at both a PV site-level and the inverter-level. These differing levels of system fidelity have varying levels of heat and power management complexity. A utility-scale inverter solar gain model has been developed, leveraging previously developed performance parameters to investigate inverter performance and cumulative damage. The incident solar gain is determined by a transient energy balance, as the difference between incident irradiance and heat loss. The model approximates the inverter geometry as a rectangular box constructed from AISI 316 stainless steel. A sensitivity analysis was also performed to assess the model's response to assumed parameters due to a lack of available information. This model also does not account for internal heat generation and cooling system heat rejection, which will be the focus of

another study. Additionally, this work assumes the inverter is unobstructed from shading and thermal radiative forcing of nearby structures. Finally, this work examines data collected from twelve, 500kW inverters from a utility-scale PV site to apply this analysis. Each inverter has a meteorological test station located adjacent to it.

II. Methodology

A. Solar Gain Inverter Model

Inverter surface temperatures were determined by considering thermal energy exchange between the inverter with its ambient environment through heat transfer modes of convection, radiation and conduction. In desert environments, the rate of change of ambient, as well as inverter system temperatures can be significant warranting a non-steady-state energy balance.

For simplicity, the utility-scale inverter was modeled as a rectangular box with four vertical walls and one horizontal wall. A control volume was assessed across each of the five respective walls according to Fig. 1, where the resulting energy balance is expressed as:

$$\rho_{Inv} V_{Side} C_{p,Inv} \frac{dT_{Surf}}{dt} = \dot{Q}_{sw} - \dot{Q}_{lw} - \dot{Q}_{Conv} - \dot{Q}_{Cond} \quad (1)$$

such that:

$$\dot{Q}_{sw} - \dot{Q}_{lw} - \dot{Q}_{Conv} - \dot{Q}_{Cond} = \dot{Q}_{sw} - \dot{Q}_{Out} = \dot{Q}_{SG} \quad (2)$$

where T_{Surf} is the outer wall surface temperature, $\dot{Q}_{SG}$ is the solar gain contribution. In Eqn. (1), ρ_{Inv} is the density and C_p is the heat capacity of the inverter wall material, where for this study the material properties were taken to be of a common AISI 316 stainless steel alloy.

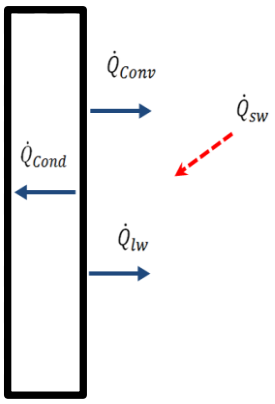

Fig. 1. Heat transfer energy exchange at the inverter wall

In Eqn (1), $\dot{Q}_{lw}$ is heat transfer due to long-wave radiation, $\dot{Q}_{sw}$ is heat transfer due to short-wave radiation, $\dot{Q}_{Cond}$ is conduction, and $\dot{Q}_{Conv}$ is convection heat transfer with heat removal contributions due to both natural and forced convection, which can be determined through Newton's law of cooling.

$$\dot{Q}_{conv} = (h_f + h_{NC}) A_{Surf} (T_{Surf} - T_{Amb}) \quad (2)$$

For external flow over a flat surface, Nusselt number is calculated as the ratio of convective to conductive heat transfer across the boundary, which is determined from appropriate forced and natural convection empirical correlations for respective vertical or horizontal walls. Many of the correlations used in this analysis, can be found in Incropera DeWitt [21].

$$NU_{L_C} = \frac{hL_C}{k} \quad (3)$$

To compute the forced convection component, a constant wind speed of 6 m/s was used, pertaining to average values for the site's location.

The short-wave radiation incident on each of the four vertical walls of the inverter can be computed from Eqn. (4), where ϕ is equal to $\dot{Q}_{GHI}$ irradiance, comprised of direct-normal, diffuse and ground reflective radiative contributions.

$$\dot{Q}_{sw} = \sum_i \alpha \phi_i A_i \quad (4)$$

$$\phi = \dot{Q}_{DNI} + \dot{Q}_{Diffuse} + \dot{Q}_{GR} \quad (5)$$

For the vertical surfaces of the inverter, $\dot{Q}_{DNI}$ was determined from a dynamic global to direct irradiance conversion model by Perez et. al. [20]. The diffuse component was adapted from a model developed by Klucher [23]:

$$\dot{Q}_{Diffuse} = \dot{Q}_{DHI} \left(\frac{1+cos(\beta_{wall})}{2}\right) \times \left[1 + F sin^3\left(\frac{\beta_{wall}}{2}\right)\right] [1 + cos^2\psi \, sin^3 Z] \quad (6)$$

such that:

$$F = 1 - \left(\frac{\dot{Q}_{DHI}}{\dot{Q}_{GHI}}\right)^2 \quad (7)$$

$$\psi = cos(\beta_{wall}) cos(Z) + sin(\beta_{wall}) sin(Z) cos(\theta_{Sun} - \theta_{wall}) \quad (8)$$

In the aforementioned equations, β_{wall} is the tilt angle of each respective wall, Z is the zenith angle, θ is the azimuth angle, and $\dot{Q}_{DHI}$ is the direct horizontal irradiance, computed as:

$$\dot{Q}_{DHI} = \dot{Q}_{GHI} - \dot{Q}_{DNI} \cos(Z) \quad (7)$$

To compute $\dot{Q}_{DNI}$ and $\dot{Q}_{Diffuse}$, latitude, longitude, altitude, as well as date and time values were required. For the ground

reflectance contribution $\dot{Q}_{GR}$, this work used a model by Loutzenhiser et. al. [20]:

$$\dot{Q}_{GR} = \dot{Q}_{GHI}\ \rho_{Surf}\left(1 - cos(\beta_{wall})\right) \quad (8)$$

For the top horizontal wall, ϕ was taken to be equal to $\dot{Q}_{GHI}$. For long-wave radiation component, the outer inverter surfaces were assumed to act as gray bodies with long wave electromagnetic energy radiation computed using a model adapted from Jones and Underwood [25].

$$\dot{Q}_{lw} = A\sigma\left[\varepsilon_{Surf}T_{Surf}^4 - \left(\frac{1+cos(\beta_{wall})}{2}\varepsilon_{sky}T_{sky}^4\right) - \left(\frac{1-cos(\beta_{wall})}{2}\varepsilon_{Ground}T_{Ground}^4\right)\right] \quad (9)$$

In this investigation we assume the inverter is not overlooked by adjacent structures and that the ground temperature is approximately equal to the ambient temperature. Therefore the radiative view factor facing the sky has a view factor of $\left(1 + cos(\beta_{wall})\right)/2$, and the portion facing the ground has a view factor of $\left(1 - cos(\beta_{wall})\right)/2$. Values for the radiation parameters in Eqn. (3) were taken from Schott [26] where ε_{Sky} = 0.95 and $T_{\text{Sky}} = T_{\text{amb}} - \delta T$ for clear-sky conditions, and ε_{Sky} = 1 and for overcast conditions, $\varepsilon_{\text{Ground}}$ = 0.95.

The final solar gain heat input for the entire inverter was determined as the sum of $\dot{Q}_{SG}$ for each of the respective walls. To determine the inner inverter temperature T_{In}, another energy balance was performed across the volume of the inverter space, with air as the ambient fluid and the inverter surface temperatures computed as boundary conditions, through the aforementioned calculations.

$$\rho_{In,Air}V_{In,Air}C_{p,In,Air}\frac{dT_{In}}{dt} = \sum_{i=1}^{5}\left(\dot{Q}_{Conv,In}\right)_i \quad (10)$$

Here, the air within the inverter was approximated to be still and well-mixed, which was validated by a subsequent natural convection boundary layer thickness formulation [21] for each respective inner surface:

$$\delta_{L_C,NC} = \frac{6L_C}{\left(Gr_{L_C}/_4\right)^{1/4}} \quad (11)$$

where Gr_{L_C} is the computed Gashoff number and $\delta_{L_C,NC}$ was found to be respectively less than 0.6 inches, validating the well-mixed temperature approximation for a relatively large interior inverter volume.

The time derivatives in the computational program were solved using Euler's method to solve for each respective temperature as a function of time. In Eqn. (12), t_{step} represents the time step between each data point.

$$T_{In}(t+1) = T_{In}(t) + t_{step}\frac{dT_{In}}{dt} \quad (12)$$

B. Normalized Parametric Analysis

To evaluate inverter performance and reliability as a result of solar gain, analysis from Haeberlin and Beutler [9], was adapted based on IEC standard 61724 [16], to assess inverter energy production, solar resource and the overall impact on system losses due to solar gain heating. The performance parameters below include the reference yield, equal to the ratio of in-plane irradiance to the reference PV irradiance; G_o (1000W/m^2). The array and final yield are ratios of DC and AC output energy to nameplate power of each respective installed PV array.

Reference Yield: $$Y_r = \frac{G_{meas}}{G_o} \quad (13)$$

Array Yield: $$Y_a = \frac{E_{DC}}{P_o} \quad (14)$$

Final Yield: $$Y_f = \frac{E_{AC}}{P_o} \quad (15)$$

Performance Ratio: $$PR = \frac{Y_f}{Y_r} \quad (16)$$

Inverter Efficiency: $$\eta_{Inv} = \frac{Y_f}{Y_a} \quad (17)$$

where E_{DC} and E_{AC} are respective DC and AC energy computed over a one-day period.

C. PV Utility-Scale Application

Outdoor measurements for a utility-scale PV plant have been collected over a twenty four hour period, where clear-sky conditions were present, and annual average wind speed and humidity values were observed. As shown in Fig. 1, the PV site contains inverters denoted within twelve of the boxes.

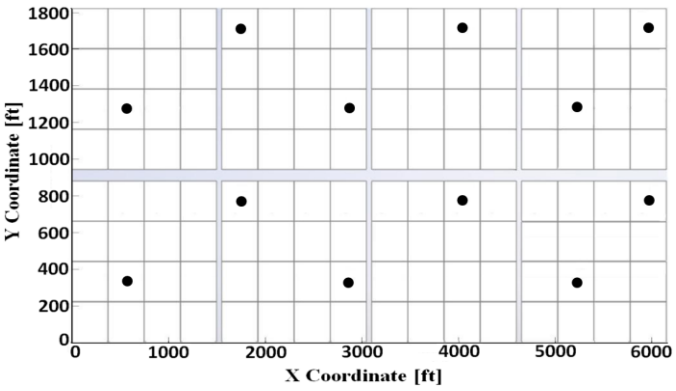

Fig. 2. PV plant layout with inverter and meteorological stations indicated by shaded circles.

Data was collected from the twelve inverters and corresponding MET stations indicated on the map in Fig. 2. Sensor errors were accounted for by evaluating clear-sky data, during different time-periods, against respective mean values

to determine offset error correction factors. To properly account for thermal inertia and evaluate heat losses, night time data during the 24 hour period was also included.

II. Results

Cumulative solar gain contributions, as well as inverter efficiency values for each of the twelve respective inverters, over a one-day period are presented in Fig. 3. One-minute data resolution was used for this particular study.

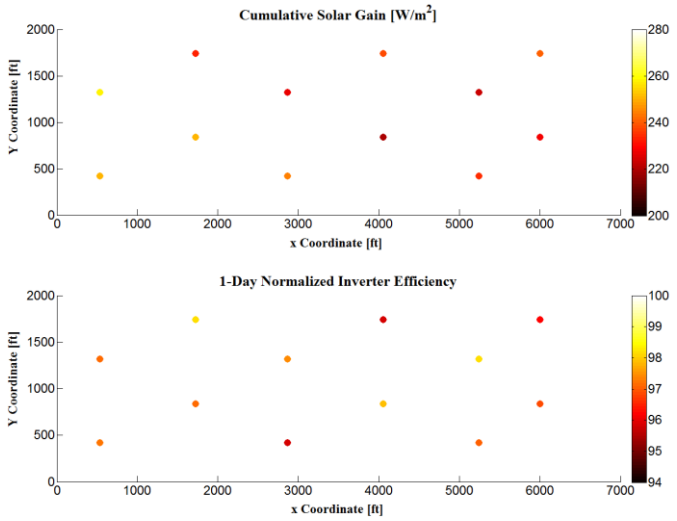

Fig. 3. Data Distribution maps for PV plant inverter cumulative solar gain and normalized inverter efficiencies, for twelve inverters, over a 24 hr. period.

Next, the values from both plots of Fig. 3 were sorted according to descending values of cumulative solar gain with the results shown in Fig. 4. A linear regression analysis was applied to this data set, which suggests an overall negative $3.6\text{x}10^{-4}$ $[\text{W/m}^2]^{-1}$ normalized efficiency correspondence with solar gain for all twelve inverters across the site.

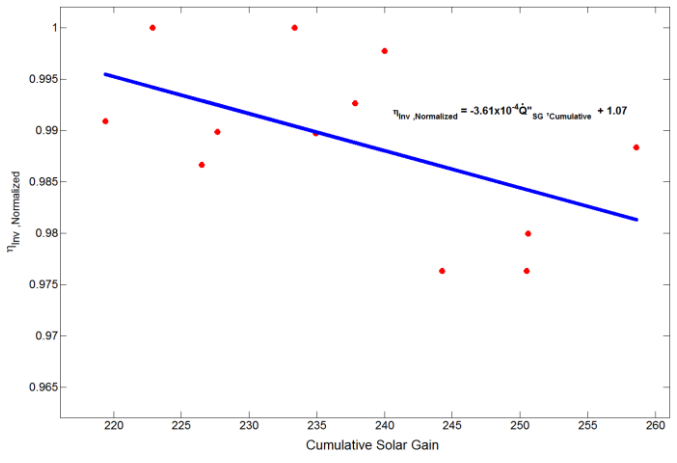

Fig. 4. PV plant inverter cumulative solar gain vs. inverter efficiency correspondence over a 24 hr. period.

Total inverter thermal flux values can be seen in Fig. 5 for the inverter with calculated median cumulative solar gain input values. Since $\dot{Q}_{DNI}$ was found to change differently for each respective outer inverter surface, $\dot{Q}_{SW,Tot}$ was found to deviate from that of the total irradiance $\dot{Q}_{Irr}$. Over the course of the day, inverter heat losses were found to be less than $\dot{Q}_{SW,Tot}$ until about 1:30PM, where they then became dominant, causing a reduction in solar gain.

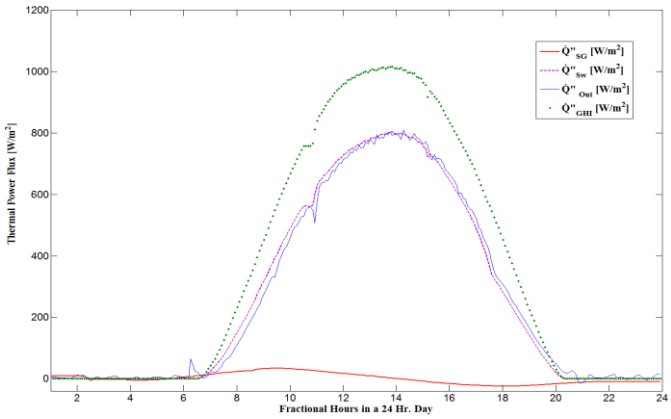

Fig. 5. Incident solar GHI values over a 1-day clear-sky period, along with heat flux values due to incident short wave radiation, heat loss and resultant solar gain heat flux.

The modeled inner inverter temperature was compared against the measured inner inverter temperature with correspondence shown in Fig. 6. For this particular inverter, the RMSE was found to be 6.1%, which suggests a good correspondance between the model and measured inverter temperatures. This RSME value was found to vary by 5.1% for the other eleven inverters, however further study is required to validate the trends of this small data set with the other inverters at the site.

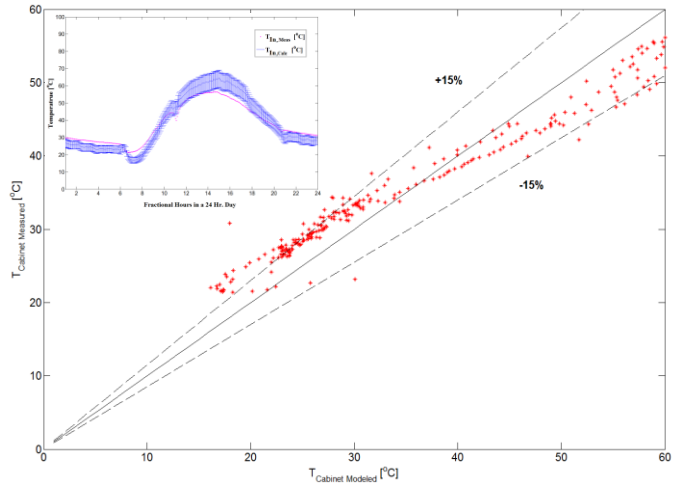

Fig. 6. Measured and calculated cabinet temperature for the median cumulative solar gain inverter, with 24 hr. comparison between both data sets in top-right plot containing computational error bars.

Many of the parameters in this transient thermal model were either measured or can be found on the inverter manufacturer's data sheet. However, some parameters were not accessible, which included the temperature and emissivity of the sky T_{Sky}, ε_{Sky}, and ground T_{Ground} , $\varepsilon_{\text{Ground}}$, as well as the material type for the inverter casing, where properties were assumed for α_{Surf} , k_{wall} , ρ_{wall} and $C_{p,wall}$. A sensitivity analysis was performed for each these parameters via a set of "one-off" analyses where one parameter was varied over a respective range of possible stainless steel alloy property values, while keeping all other parameters fixed. Internal inverter temperatures, and a corresponding measured temperatures RSME error, were then calculated. The results of Fig. 7 demonstrate that α_{Surf} has an optimally low RSME value at 0.65, however this property has been found to vary over time with degradation of surface materials and coatings on metals [24].

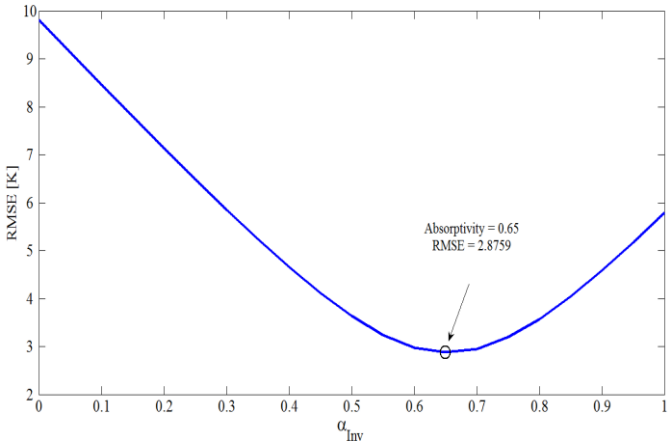

Fig. 7. Absorptivity sensitivity analysis over a range of α = 0–1, with an RMSE minimum reached at an α value of 0.65.

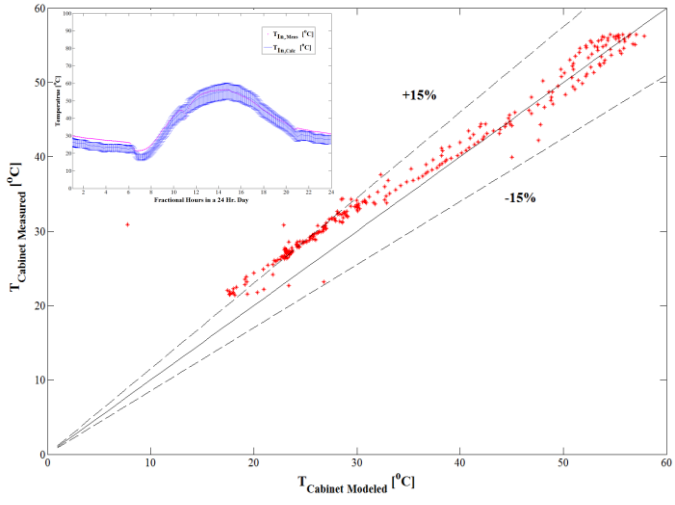

Fig. 8. Optimized model measured and calculated cabinet temperature for the median cumulative solar gain inverter with, 24 hr. comparison between both data sets in top-right plot containing computational error bars

The results of the other studies found respective optimal values of 26.5 W/m-K, 7480 kg/m^3 and 490 J/kg-K, with RMSE standard deviations of only 0.16, 0.04 and 0.03, indicating that the model has the highest degree of sensitivity to α_{Cab} for these four parameters. Justification can be attributed to its direct impact on the computations of $\dot{Q}_{sw}$. Next, imposing these optimal parameters back into the original model we find a 39% average reduction in RMSE.

III. Conclusions

A new model for evaluating inverter performance based on solar gain is presented that computed inner inverter temperatures, over a one-day, clear-sky period, to within 6.1% error. Further analysis revealed as high as 22.9% model sensitivity to surface absorptivity, which has a direct impact on the ability for incident short wave radiation to be absorbed. Overall, the results of this study show an overall negative $3.6\text{x}10^{-4}$ $[\text{W/m}^2]^{-1}$ normalized inverter efficiency correspondence with solar gain over the one-day time period. However further research over an extended time period; with the inclusion a larger data set of inverters is required to validate these findings. The heat transfer model will also need to be further developed to include heat transfer contributions due to internal heat generation and heat removal from on-board cooling systems. These contributions, such as DC line voltage, can also impact inverter efficiency that will also require further fundamental examination beyond the analysis presented here.

Acknowledgement

Sandia National Laboratories is a multi-program laboratory managed and operated by Sandia Corporation, a wholly owned subsidiary of Lockheed Martin Corporation, for the U.S. Department of Energy's National Nuclear Security Administration under contract DE-AC04-94AL85000.

References

[1] N. Sorensen, E. Thomas, M. Quintana, S. Barkaszi, A. Rosenthal, A. Zhang, and S. Kurtz, "Thermal study of inverter components", *37th IEEE PV Spec. Conf.*, Area 9, 2012.

[2] M. Reno, J. Stein, "Photovoltaic inverter: Thermal characterization to identify critical components," 2012.

[3] M. Catelani, L. Ciani, E. Simoni, "Photovoltaic inverter: Thermal characterization to identify critical components," *XX IMEKO World Congress – Metrology for Green Growth*, Busan, Republic of Korea 2012.

[4] V. Smet, and F. Forest, "Ageing and failure modes of IGBT modules in high-temperature power cycling", *IEEE Trans. On Indus. Elecs.*, 58, No. 10, 2011.

[5] D. Benning, J. Reichl, A. Hefner, M. Hernandez, C. Ellenwood and J-S. Lai, " High speed IGBT module transient thermal response measurements for model validation", *Ind. App. Conf. 38th IAS Annual Meeting*, 2003.

[6] P. Zhang, Y. Wang, W. Xiao and W. Li, "Reliability evaluation of grid-connected photovoltaic power systems", IEEE Trans. On Sus. Energy 3, No. 3, 2012.

[7] J. He, M. Shaw, J. Mather and R. Addison, "Direct measurement of the time-dependent evoluation of stress in silicon devices and solder interconnections in power assemblies", Ind. App. Conf., *38th IAS Annual Meeting*, 2003.

[8] B. Marion, J. Adelstein, K. Boyle, H. Hayden, B. Hammond, T. Fletcher, B. Canada, D. Narang, A. Kimber, L. Mitchell, G. Rich and T. Townsend, "Performance parameters for grid-connected PV systems", *31st IEEE PV Spec. Conf.*, 2005.

[9] H. Haeberlin, Ch. Beutler, "Normalized representation of energy and power for analysis of performance and on-line error detection in PV-systems," *13th EU PV Conference on Solar Energy*, Nice, France, 1995.

[10] K. Thongpao, P. Sripadungdungtham, P. Raphisak, K. Sriprapha, and E. Hattha, "Outdoor performance of polycrystalline and amorphous silicon solar cells based on the influence of irradiance and module temperature in Thailand", *IEEE 28th PV Spec. Conf.*, 2000.

[11] S. Ransome, "Modelling inaccuracies of PV energy yield simulations," IEEE 33rd PV Spec. Conf., 2008.

[12] G. Pfister, R. McKenzie, J. Liley and A. Thomas, "Cloud coverage based on All-Sky imaging and its impact on surface solar irradiance", *J. Appl. Meteor.*, **42**, 1421–1434, 2003.

[13] E. Kern, E. Gulachenski and G. Kern, "Cloud effects on distributed photovoltaic generation: Slow transients at the Gardner, Massachusetts photovoltaic experiment", *IEEE Trans. On Energy Conv.*, 4, No. 4, 1989.

[14] P. Mathiesen and C. Collier, "Characterization of irradiance variability using a high-resolution, cloud-assimilating NWP", *World Renewable Energy Forum*, 2012.

[15] M. Lave and J. Kleissl, "Cloud speed impact on solar variability scaling – Application to the wavelet variability model", *J. Solar Energy*, vol. 91, pp. 11-21, 2013.

[16] IEC Standard 61724, "Photovoltaic system performance monitoring - Guidelines for measurement, data exchange and analysis", *International Electrotechnical Commission*, Geneva, Switzerland, 1998.

[17] M. Hollander, D. Wolfe, "Nonparametric statistical methods," New York, Wiley, 1973.

[18] R. Sibson, "A brief description of natural neighbor interpolation (Chapter 2", In V. Barnett, Interpolating Multivariate Data, Chichester: John Wiley. pp. 21-36, 1981.

[19] P.G. Loutzenhiser, H. Manz, C. Felsmann, P.A. Strachan, T. Frank and G.M. Maxwell, "Empirical validation of models to compute solar irradiance on inclined surfaces for building energy simulation," *Solar Energy*, vol. 81, pp. 254-267, 2007.

[20] R. Perez, P. Ineichen, E. Maxwell, R. Seals and A. Zelenka, "Dynamic Global-to-Direct Irradiance Conversion Models," *ASHRAE Transactions-Research Series*, pp. 354-369, 1992.

[21] F. P. Incropera and D.P. Dewitt, "Fundamentals of heat and mass transfer," Danvers, Massachusetts, John Wiley and Sons, 5th Ed., 2002.

[22] S.W. Churchill and H.H.S. Chu, "Correlating equations for laminar and turbulent free convection from a vertical plate," International Journal of Heat and Mass Transfer, Vol. 18, pp. 1323, 1975.

[23] T.M. Klucher, "Evaluation of models to predict insolation on tilted surfaces," *Solar Energy*, vol. 23, No. 2, pp. 111–114, 1979

[24] A. Ghosh, "Degradation of polymer/substrate interfaces – an attenuated total reflection Fourier transform infrared spectroscopy approach," M.S. Thesis, The Ohio State University, Columbus, Ohio, 2010.

[25] A.D. Jones and C.P. Underwood, "A thermal model for photovoltaic systems," *Solar Energy*, vol. 70, No. 4, pp. 349-359, 2001.

[26] T. Schott, "Operational temperatures of PV modules," *6th PV Solar Energy Conference*, pp. 392-396, 1985.